Appl. Phys. B 89, 231–234 (2007)
DOI: 10.1007/s00340-007-2778-4

Applied Physics B
Lasers and Optics

KI SOO CHANG
YOUNG MIN SONG
YONG TAK LEE✉

Stable single-mode operation of VCSELs with a mode selective aperture

Department of Information and Communications, Gwangju Institute of Science and Technology (GIST), 1 Oryong-dong, Buk-gu, Gwangju, 500-712, Republic of Korea

Received: 22 March 2007 / Revised version: 3 August 2007
Published online: 11 September 2007 •

ABSTRACT We have developed single-mode vertical-cavity surface-emitting laser (VCSELs) with a mode selective aperture (MSA) in the DBR mirror that exhibits a high-order transverse-mode filtering effect. The VCSELs with an MSA were fabricated using standard intracavity-contacted VCSEL processes without any additional steps resulting from the simultaneous formation of the MSA and current aperture via a single-step oxidation. The VCSELs fabricated with a current aperture and MSA diameter of 5 and 7 μm, respectively, exhibited a stable single-mode operation with a side mode suppression ratio of over 35 dB and a divergence angle below 10° for the entire drive current range.

PACS 42.55.Px; 85.35.Be

1 Introduction

Due to their superior characteristics and low manufacturing costs, vertical-cavity surface-emitting lasers (VCSELs) have become a standard light source in short distance optical data links, such as local area networks (LANs) and storage area networks (SANs), using a multimode fiber (MMF) as the transmission media [1]. Recently, single-mode VCSELs have attracted great interest in high bit rate data transmission (over 10 Gbps) applications, as well as many other applications where a relatively low output power with a high quality optical beam is required, such as board-to-board and chip-to-chip free space optical interconnects [2], laser absorption spectroscopies [3], laser-based optical mouse sensors [4], and chip-scale atomic clocks [5]. To obtain a stable single-transverse-mode operation for oxide-confined VCSELs, the oxide aperture diameter should typically be reduced to less than 3 μm due to the large effective index step induced by the low refractive index of the Al-oxide layer. Unfortunately, a small aperture causes an increased series resistance and beam divergence, which limits the high speed operation and optical efficiency, respectively. Furthermore, the fabrication of a uniform and reproducible single-mode VCSEL array with a small oxide aperture is difficult due to the difficulty in controlling oxidation precisely. To date, several methods have been developed to obtain a single-transverse-mode operation with a larger oxide aperture diameter: surface relief etching [6], extended monolithic optical cavities [7], a combination of an implant and oxide aperture [8], an antiresonant reflecting optical waveguide (ARROW) structure [9], and a photonic crystal structure [10]. However, these methods require multiple process steps or growth interruption and regrowth steps, which hamper low cost and high yield manufacturing. A patterned thin layer on the top distributed Bragg reflector (DBR) structure can also promote a fundamental mode operation, but in a limited range of driving currents [11].

In this article, we report a simple and robust technique for obtaining a stable single-transverse-mode operation of an oxide-confined VCSEL over the entire drive current range by introducing a mode selective aperture (MSA) in the top DBR to suppress the high-order modes.

2 Device structure and fabrication

Figure 1 shows a schematic illustration of the proposed oxide-confined VCSEL with an MSA to suppress the high-order modes. The MSA, formed naturally in the top DBR during the selective oxidation step for the current aperture (CA) formation, provides a large optical loss in the outer region of the top mirror. If the MSA diameter is larger than the fundamental mode width and smaller than the high-order mode width, only the lasing threshold for the high-order mode becomes high. Thus, a VCSEL with an MSA can maintain a stable fundamental mode operation. The MSA diameter

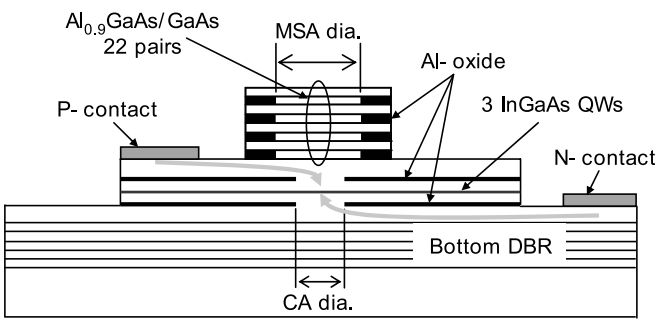

FIGURE 1 Schematic illustration of the oxide-confined VCSEL with a mode selective aperture (MSA) for a high-order mode suppression

✉ Fax: +82-62-970-3128, E-mail ytlee@gist.ac.kr

can be easily controlled by varying the first mesa diameter, which enables the simultaneous formation of MSA and CA via single step oxidation. We measured the near-field profile to investigate the spatial intensity distribution of the transverse modes in the VCSEL. Figure 2 shows measured near-field profiles for a VCSEL without MSA and with CA of 5 μm in diameter. Only a Gaussian-like fundamental mode is excited at slightly above the threshold current, while a high-order transverse mode exhibiting an intensity dip in the center was excited at a bias current of $2I_{th}$. The full width at half maximum (FWHM) of the fundamental mode and high-order mode are 4.3 and 8.4 μm, respectively. In order to experimentally confirm the validity of the proposed concept, VCSELs with MSAs of 9 and 7 μm and a fixed CA of 5 μm in diameter were fabricated and characterized.

The epitaxial layer structure was grown using the DCA P600 solid source molecular beam epitaxy (MBE) system. The top and bottom DBR mirrors consist of 23 and 30.5 pairs of quarter-wavelength-thick GaAs-$Al_{0.9}Ga_{0.1}As$ layers, respectively. The resonator cavity consists of three 80 Å-thick $In_{0.2}Ga_{0.8}As$ quantum wells with 100 Å-thick GaAs barriers surrounded by $Al_{0.3}Ga_{0.7}As$ spacers to form a single wavelength cavity. The cavity is bounded on each side by p- and n-doped $Al_{0.98}Ga_{0.02}As$ oxidation layers, followed by 5/4 λ-thick p- and n-doped GaAs contact layers. Because the 45 nm-thick $Al_{0.98}Ga_{0.02}As$ oxidation layers are located between the node and antinode of the standing wave pattern, the epitaxial layer structure is not yet optimized for a high-power single-mode operation [12].

The device processing began with the formation of cylindrical mesas of 14 and 12 μm, respectively, corresponding to the MSAs with 9 and 7 μm diameters, by dry etching the top DBR down to the p-GaAs contact layer. Next, the cylindrical mesas with a diameter of 54 μm, whose centers coincide with the first mesas, were defined. The p-GaAs contact layer, two $Al_{0.98}Ga_{0.02}As$ oxidation layers, and the cavity were etched until the n-GaAs contact layer was exposed. At the photolithography step to define the second mesas, a careful alignment procedure was needed because misalignment between first and second mesas may degrade the device performance. Typically, we can obtain an alignment accuracy of ±0.3 μm or better using a manual mask aligner, and this level of alignment accuracy is sufficient to meet the required tolerance for optimum device performance. After mesa etching, the CAs and MSAs were formed simultaneously in a wet thermal oxidation furnace at a temperature of 400 °C for 118 min. The p-contact metal (Ti/Pt/Au) and n-contact metal (Ni/Au/Ge/Ni/Au) were deposited on the p- and n-GaAs contact layers, respectively. To reduce the current crowding at the oxide aperture rim, and to favor lasing in the fundamental mode, we fabricated asymmetric intracavity-contacted VCSELs [13]. The p- and n-contacts are restricted to the opposite sides of the mesas, as shown in Fig. 1. Standard intracavity-contacted VCSEL processing was used to fabricate VCSELs with MSA without additional process steps due to the simultaneous formation of MSA and CA via single step oxidation by properly controlling the mesa diameters.

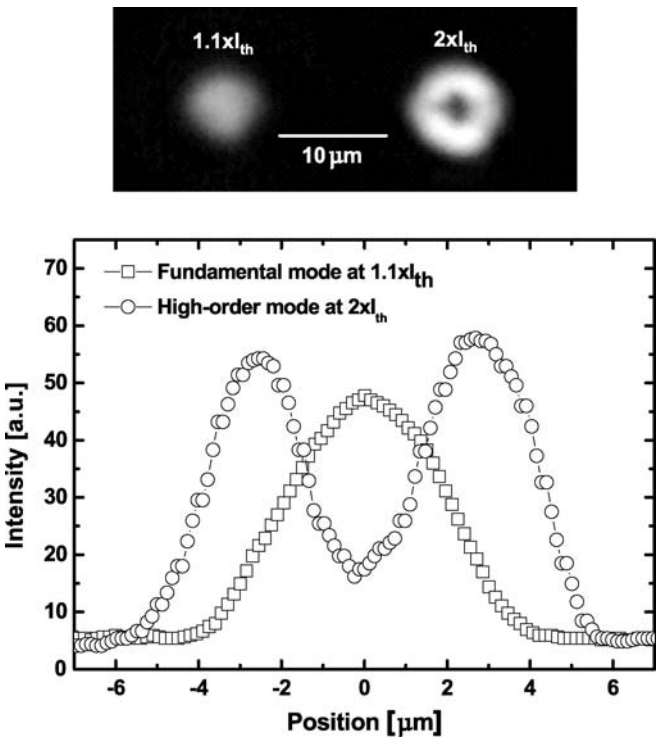

FIGURE 2 Measured near-field intensity distribution for a VCSEL without MSA and with CA of 5 μm in diameter

3 Results and discussion

Figure 3 shows the cw lasing spectra and light output characteristics of the fabricated VCSELs with MSAs of 9 and 7 μm in diameter at room temperature. The threshold current and differential quantum efficiency for the VCSEL with an MSA diameter of 9 μm are 0.9 mA and 0.25, respectively, and it operates in the fundamental mode up to 2 mA, then becomes multimode for higher currents. For the VCSEL with an MSA diameter of 7 μm, a completely stable single-mode operation was achieved with a side mode suppression ratio of 35 dB over the entire drive current range. The threshold current and differential quantum efficiency are 1.1 mA and 0.19, respectively. For the VCSEL with the smaller MSA, 7 μm, the threshold current increased slightly and the differential quantum efficiency decreased. This result can be attributed to the increase of optical loss by MSA not only for high-order transverse modes, but also for the fundamental mode.

In addition to the light output and spectra measurements, the near-field pattern (NFP) and far-field pattern (FFP) measurements are also required to determine the actual emission profile. The measured NFP and FFP for various driving currents are shown in Figs. 4 and 5, respectively. For the VCSEL with an MSA diameter of 9 μm, the NFP and FFP are Gaussian-like from the threshold to 2 mA, and then progresses to a non-Gaussian-like pattern, which indicates the excitation of high-order modes, as the bias current increases. The measured NFP and FFP for the VCSEL with a 7 μm MSA diameter are Gaussian-like over the entire current range, which again confirms the single-transverse-mode operation. For the VCSEL with an MSA diameter of 9 μm, the FWHM of the far-field angle starts from approximately 9° at the threshold current and remains almost constant during the single-mode

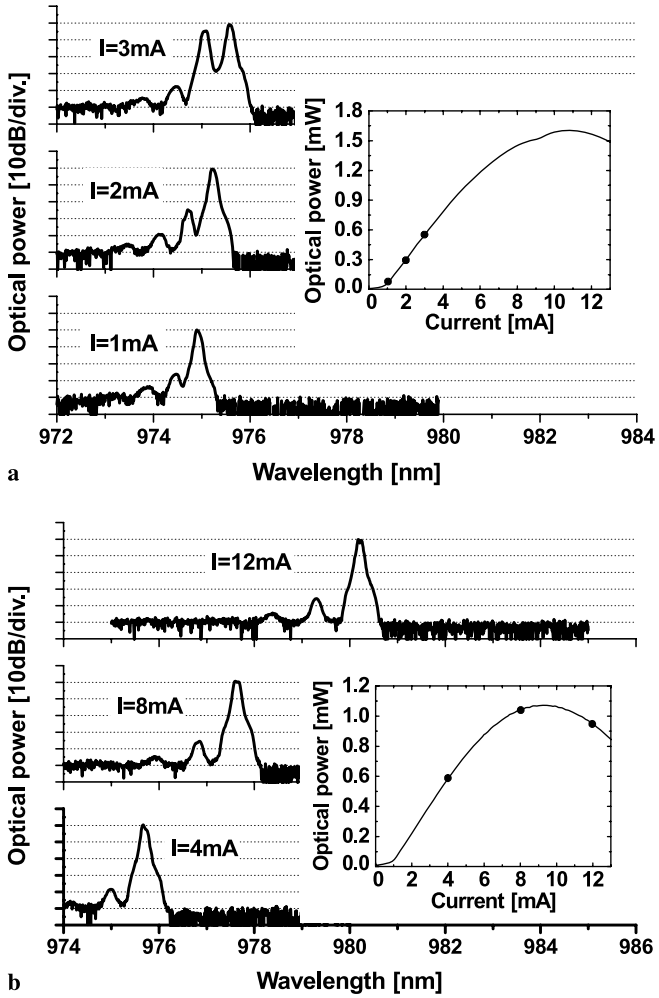

FIGURE 3 CW lasing spectra for VCSELs with a fixed CA diameter of 5 μm, and MSA diameters of (**a**) 9 and (**b**) 7 μm, respectively. *Inset*: output power vs. bias current characteristics

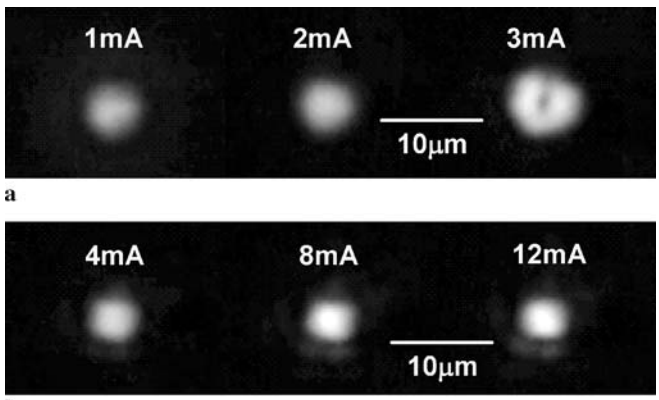

FIGURE 4 The measured near-field images for VCSELs with MSA diameters of (**a**) 9 and (**b**) 7 μm at different current levels

operation. However, it increases abruptly with the current after the high-order transverse modes are excited. In contrast, for the VCSEL with an MSA diameter of 7 μm, the FWHM of the far-field angle only broadens by approximately 14% and remains below 10° over the entire current range. This far-field angle behavior agrees well with the spectra measurements.

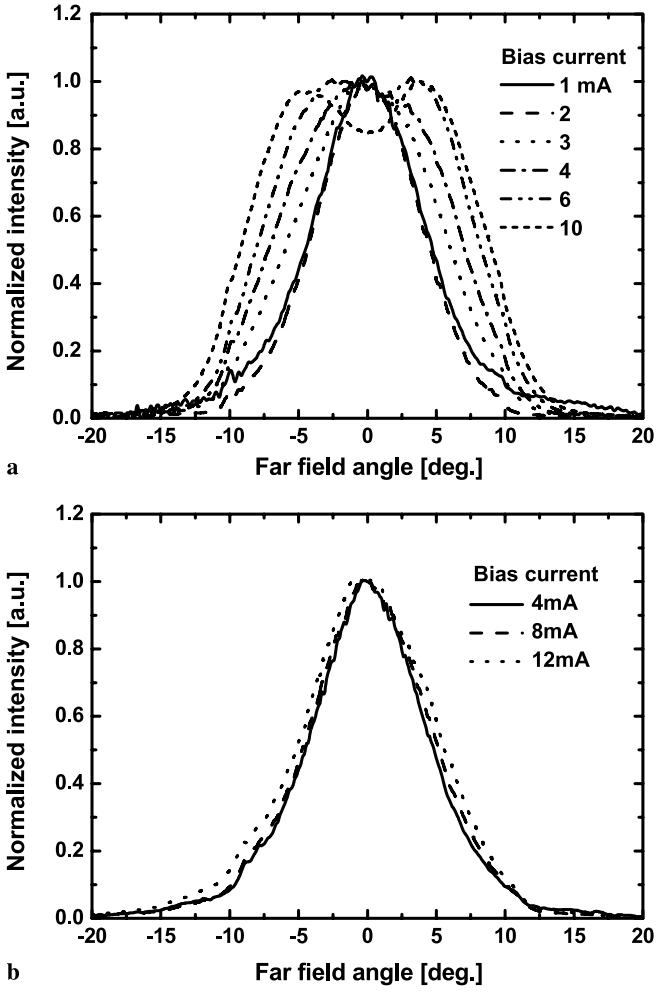

FIGURE 5 The measured far-field profiles for VCSELs with MSA diameters of (**a**) 9 and (**b**) 7 μm at different current levels

The single-mode operation for the entire drive current range and reduced output power for the VCSEL with the smaller MSA indicate that the maximum single-mode output power can be increased by optimizing the MSA diameter relative to the CA diameter. To minimize the optical loss for the fundamental mode, we need to estimate the modal loss. In addition, the thickness and position optimization of the oxidation layer to reduce the effective index step should also lead to improving single-mode power. These efforts are underway and we would like to discuss the theoretical and experimental results elsewhere.

4 Conclusion

The stable single-mode operation of a VCSEL with a side mode suppression ratio of 35 dB and a divergence angle below 10° was achieved over the entire drive current range by introducing a mode selective aperture as a high-order mode filter in the top DBR mirror. Standard intracavity-contacted VCSEL processes were used without any additional steps to fabricate single-mode VCSELs with large current aperture, which verified the advantage of this method. This technique is considered applicable to the low cost and high yield manufacturing of stable single-mode VCSELs.

ACKNOWLEDGEMENTS This work was supported by MOST through the TND project.

REFERENCES

1 J.A. Tatum, J.K. Guenter, Proc. SPIE **4994**, 1 (2003)
2 Å. Haglund, C. Carlsson, J.S. Gustavsson, J. Halonen, A. Larsson, Proc. SPIE **4649**, 272 (2002)
3 H.P. Zappe, M. Hess, M. Moser, R. Hovel, K. Gulden, H.-P. Gauggel, F. Monti di Sopra, Appl. Opt. **39**, 2475 (2000)
4 R. Szweda, III–Vs Rev. Adv. Semicond. Mag. **17**, 2 (2004)
5 S. Knappe, V. Shah, P.D.D. Schwindt, L. Hollberg, J. Kitching, L.-A. Liew, J. Moreland, Appl. Phys. Lett. **85**, 1460 (2004)
6 H.J. Unold, S.W.Z. Mahmoud, R. Jager, M. Grabherr, R. Michalzik, K.J. Ebeling, IEEE J. Sel. Top. Quantum Electron. **7**, 386 (2001)
7 H.J. Unold, S.W.Z. Mahmoud, R. Jager, M. Kicherer, M.C. Riedl, K.J. Ebeling, IEEE Photon. Technol. Lett. **12**, 939 (2000)
8 E.W. Young, K.D. Choquette, S.L. Chuang, K.M. Geib, A.J. Fisher, A.A. Allerman, IEEE Photon. Technol. Lett. **13**, 927 (2001)
9 D. Zhou, L.J. Mawst, Appl. Phys. Lett. **76**, 1659 (2000)
10 A.J. Danner, J.J. Raftery, P.O. Leisher, K.D. Choquette, Appl. Phys. Lett. **88**, 091 114 (2006)
11 R.M. Wurtemberg, P. Sundgren, J. Berggren, M. Hammer, M. Ghisoni, E. Odling, V. Oscarsson, J. Malmquist, Appl. Phys. Lett. **85**, 4851 (2004)
12 A.E. Bond, P.D. Dapkus, J.D. O'Brien, IEEE Photon. Technol. Lett. **10**, 1362 (1998)
13 G. Verschaffelt, W. van der Vleuten, M. Creusen, E. Smalbrugge, T.G. van de Roer, F. Karouta, R.C. Strijbos, J. Danckaert, I. Veretenicoff, B. Ryvkin, H. Thienpont, G.A. Acket, IEEE Photon. Technol. Lett. **12**, 945 (2000)